Investigations on the Resonant Properties of a New Compact Asymmetric Single Split Resonator for Metamaterial Applications

Parackattu V. Anila[1, 2, *], Manoj Mani[1], Moolat Remsha[1], Raghavan Dinesh[1], Anju Pradeep[3], Karavila V. C. Prakash[4], and Pezholil Mohanan[1]

Abstract—This paper presents the resonant properties of a new Asymmetric Single Split Resonator (ASSR) structure for metamaterial applications. The compact uniplanar structure is an asymmetric single split ring resonator with two non-concentric rings. The prototype is fabricated on a substrate of dielectric constant 4.4, loss tangent 0.025, and thickness 1.6 mm and analyzed based on reflection and transmission coefficients and unit cell simulations. The fabricated unit cell of miniaturized ASSR has a footprint area of $0.163\lambda_0 \times 0.163\lambda_0$ where λ_0 is the measured free-space wavelength corresponding to 1.63 GHz. The negative permeability meta-particle is best suited for high-performance multiband bandstop filters, sensors, and RFID applications in advanced communication systems. The paper presents the electric and magnetic responses of ASSR with its constitutive parameters for different field orientations in normal incidence.

1. INTRODUCTION

Artificial metamaterials created a new paradigm in the design of present-day high-performance electronic gadgets. The realization of Pendry's artificial magnetic media [1] by Smith et al. [2] provided the first novel structure, Split Ring Resonators (SRRs) with unusual properties. A thorough study of different metamaterials and their characteristics has been reported widely [3–6] over the last years. The key applications of metamaterials mainly exploited are antenna miniaturization, bandwidth enhancement, directivity/gain enhancement, spurious radiation suppression [7–9], etc. The researchers are very fond of making new artificial materials to keep enhancing the performance of wireless communication systems. Fedotov et al. in 2007 [10] proposed that the resonator obtained by crossing the symmetry led to extremely sharp resonance and concentrating local fields in a small volume supporting trapped modes. Later, planar arrays or frequency selective surfaces (FSS) were replaced with compact single planar asymmetry split resonators by Al-Naib et al. [11–13]. Today, wireless systems with a low profile and high selectivity are very much desired for 5G networks [14, 15] which rather implies the necessity of high-performance filters with compact structures. Metamaterial designs for absorbers, power dividers, filters, isolation, capacity, and efficiency improvement of antenna in new generation wireless communication systems [16–32] are catching the eye of industries. Various metamaterial structures such as S-shaped, triangular, CRLH transmission line based, and 2D cross embedded designs are very well explained in the above works of literature. The rapid growth and development in an advanced fifth-generation communication system signify the importance of a compact, narrow bandwidth, multiband high selective resonating meta-particle. Here, the authors present a new simple, planar, and asymmetric metamaterial structure on an FR4 substrate to design narrow multiband band-stop filters, high field RFID (Radio

Frequency Identification) tags, and sensors in advanced wireless communication systems. Analysis and experimental results are implemented. The electric and magnetic responses of ASSR with its constitutive parameters for different orientations of an external electric field $\vec{E}$ and direction of propagation $\vec{k}$ are also described. The article also compares the structure with SRR and Single Split Dual Ring SRR (SD-SRR).

2. THEORY AND DESIGN OF PROPOSED ASSR

Split ring resonators are found to be the most widely used metamaterial structures to achieve negative permeability. Due to the symmetric geometry of SRR, nonlinear behavior is found to be reduced. The increased energy density within the structure suitable for filter and RFID applications can be attained by increasing the nonlinear behavior [1] using asymmetric geometry. The asymmetry is introduced to convention SRR as in Fig. 1. The geometry of the Asymmetric Single Split Resonator (ASSR) structure is shown in Fig. 1(c) derived by shifting a closed ring within a Single Split Dual Ring SRR (SD-SRR) opposite to the split gap (Fig. 1(b)). An SD-SRR is a special form of Pendry's SRR which is considered as a combination of a broadband closed ring resonator and a split ring resonator. By [10] Fedotov and the team realized high field confinement and high Q with structures of asymmetry. The ASSR can be explained as an extreme case of SD-SRR with maximum asymmetry thereby investigating the resonant properties and local fields for SRR, SD-SRR, and ASSR. The prototypes are fabricated using photolithography on a substrate of dielectric constant 4.4, thickness 1.6 mm, and loss tangent 0.025 with a unit cell dimension of $30 \times 30 \, \text{mm}^2$. The outer radius (r_1) is 12 mm, and the width of the metallic disc (t) is 2 mm. The outer radius of the inner ring (r_2) is taken to be 7 mm, and the center to center distance between the discs is 3.15 mm. The dimensions of SRR, SD-SRR, and ASSR are selected the same and to operate in the lower frequency regime about 1.5 GHz to demonstrate the compactness. The structure is devoid of any vias and additional metallic ground planes which makes it simple, uniplanar, and easy for fabrication.
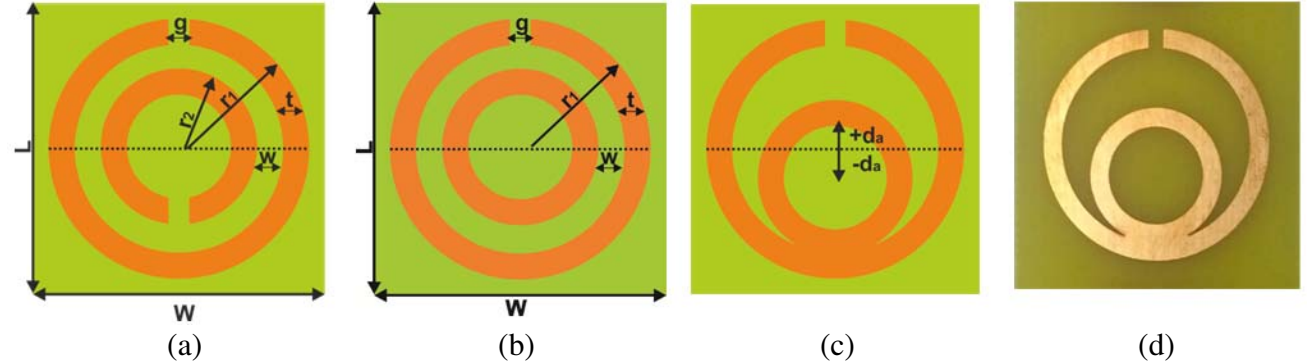

Figure 1. Evolution of Asymmetric Single Split Resonator (a) SRR — split ring resonator with dimensions $(r_1 = 12 \, \text{mm}, \, g = 2 \, \text{mm}, \, t = 2 \, \text{mm}, \, r_2 = 7 \, \text{mm} \, \text{and}, \, L = W = 30 \, \text{mm})$. (b) Single split dual ring SRR (SD-SRR) — Asymmetry is introduced by closing the inner ring. (c) ASSR-maximum offset inner ring with center to center distance of inner and outer rings = 3.15 mm. (d) Prototype on FR4.

Regarding a meta-resonator, the expression for resonant frequency is of interest. The resonant frequency of SRR is governed by the gap capacitances, inter-ring capacitance (C), and average inductance of the two rings L_{av} as in (Eqs. (1a) and (1b)). The SD-SRR is treated as a special case of SRR with C_{g_2} as infinite with zero gaps. The resonant frequency of single split dual ring resonators can be expressed as in Eqs. (2a) and (2b) where C_g is the gap capacitance and L_{eq} the total equivalent inductance (Equation (3)).

$$\omega_{\text{SRR}} = \left[L_{av} \left(C_t/4 + C_{g_1} + C_{g_2} \right) \right]^{-1/2} \tag{1a}$$

where

$$L_{av} = (L_1 + L_2)/2 \quad \text{and} \quad C_t = 2\pi C \tag{1b}$$

$$\omega_{\text{SD-SRR}} = \left[(1 + \gamma_L) \left(2\pi C_g L_{eq} \right) \right]^{-1/2} \tag{2a}$$

where

$$\gamma_L = (L_2 - M)^2 / \left(L_1 L_2 - M^2 \right) \quad \text{and} \quad \gamma_L \ll 1 \tag{2b}$$

The total equivalent inductance for SD-SRR will be

$$L_{eq} = L_1 + L_2 - 2M \tag{3}$$

where L_1 and L_2 are the self inductances of the inner and outer rings of SD-SRR, and M is the mutual inductances between these two rings which determine the inductance parameter γ_L. The ASSR can be taken as SD-SRR with maximum asymmetry where the inner closed ring of the SD-SRR is moved to the far end of the gap so that the field will be minimum at the conjunction, and the two rings form a spiral-like structure. The two rings thus contribute conduction current along the length, and the gap capacitance forms the displacement current. Hence the resonant frequency is determined only by the gap capacitance and total equivalent inductance. Also, the gap capacitance is a function of separation between the rings (w). As opposite to SRR, the inter ring capacitance has no role in resonance while the reduced capacitance effect in SD-SRR and ASSR increases the resonant frequency as $f_{\text{SRR}} < f_{\text{SD-SRR}} < f_{\text{ASSR}}$ assuming an equal average inductance. The structure is analyzed with computational electromagnetic solver CST Microwave studio, and the measurements are done using the PNA E8362B Vector Network analyzer. The simulation and measurement results are produced in the successive sections.

3. RESULTS AND DISCUSSION

All the resonant frequencies of a meta-resonator can be simply found by exciting it with a microstrip transmission line. The fabricated prototype on FR4 (Fig. 1(d)) is placed over a $50\,\Omega$ transmission line, and reflection and transmission coefficients are measured and depicted in Fig. 2. The structure shows resonant nature at $1.33\,\text{GHz}$, $2.06\,\text{GHz}$, and $3.63\,\text{GHz}$ within the 0.5–$4\,\text{GHz}$ band. To verify the ASSR unit cell characteristics, a unit cell of $30\,\text{mm} \times 30\,\text{mm}$ dimension is simulated for the infinite periodic arrangement of ASSR using CST Microwave Studio. The uniform plane wave is made incident along X-axis where the electric and magnetic fields are oriented along Y and Z axes, respectively, which is denoted by $H\|$ polarization. It is done by simulating the ASSR under unit cell simulations in CST Microwave Studio after assigning open space boundary conditions along X-axis, electric boundary along Y-axis, and magnetic boundary along Z-axis, respectively. The simulated reflection and transmission coefficients are shown in Fig. 3 together with the schematic view and excitation details. The lower
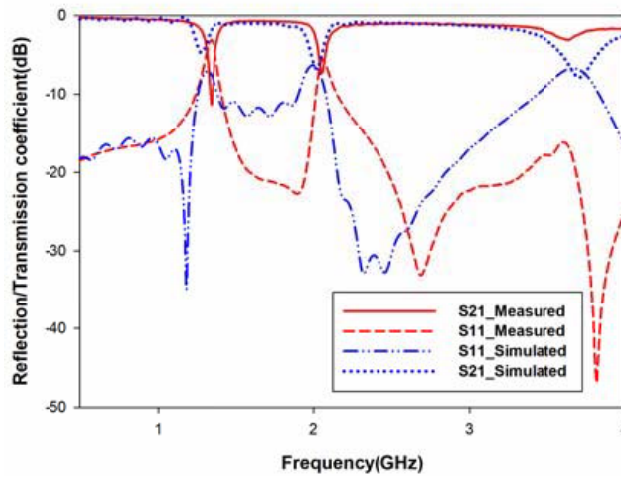

Figure 2. Measured and simulated reflection and transmission coefficients of ASSR placed over the transmission line.

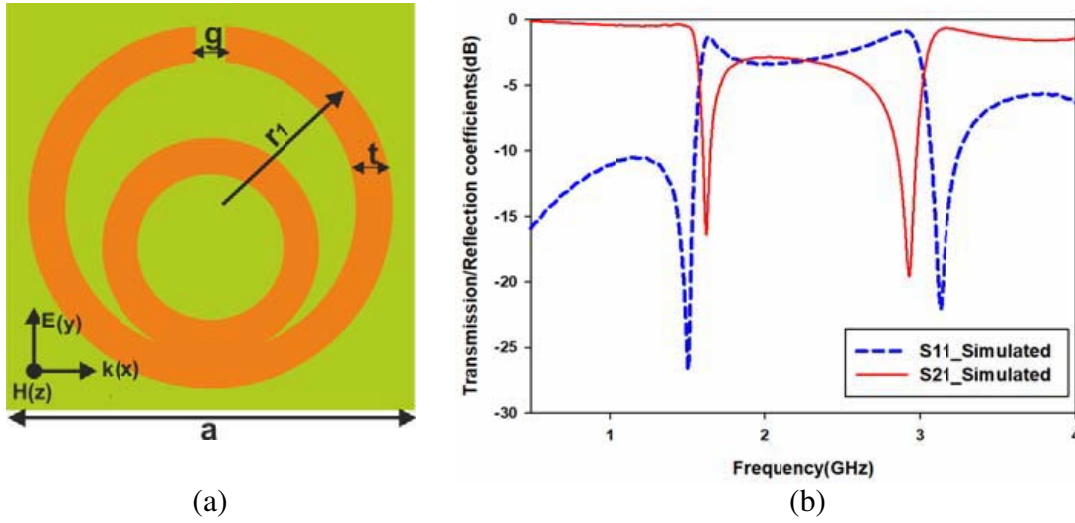(a)   (b)

Figure 3. (a) Structure of ASSR with incident electromagnetic wave polarization. (b) Simulated reflection and transmission coefficients of ASSR.
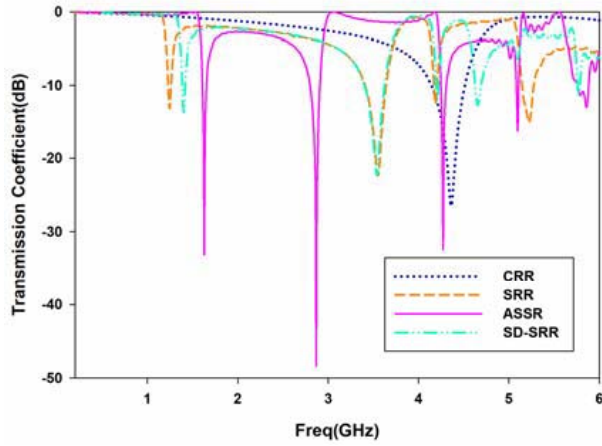

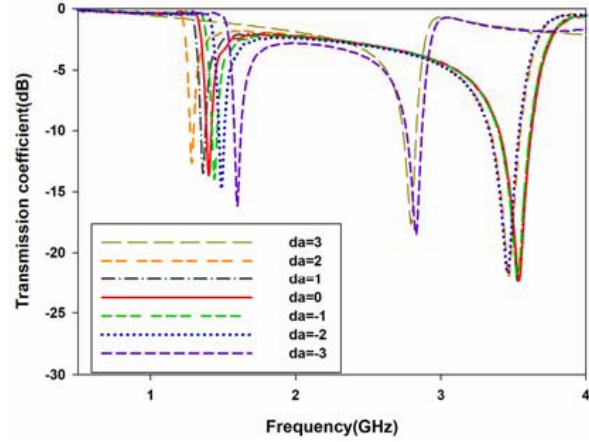**Figure 4.** Simulated transmission coefficients of (a) CRR, (b) SRR, (c) SD-SRR, (d) ASSR.

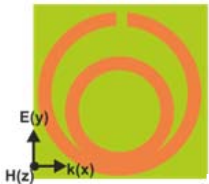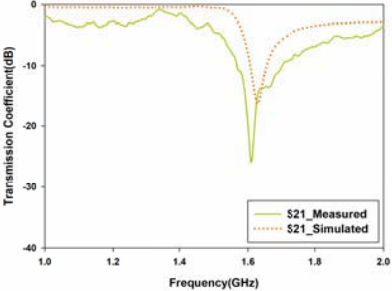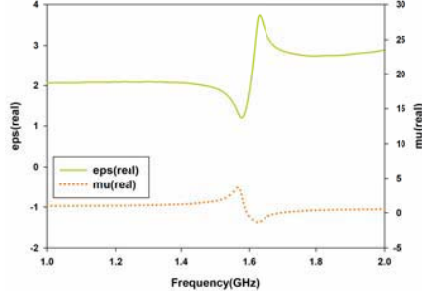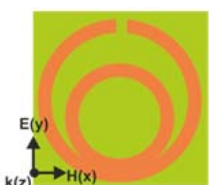**Figure 5.** Variation in transmission spectra for different values of asymmetry.
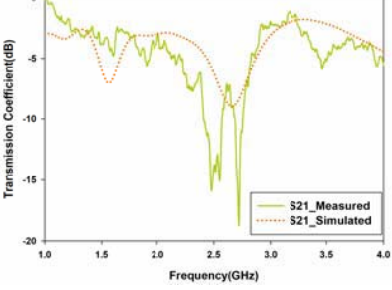
resonant frequency of 1.33 GHz in transmission line measurement is due to the additional capacitive coupling when the unit cell is placed over the transmission line. The change in measured and simulated reflection coefficients is due to the manual placing errors while the ASSR unit cell is placed on the transmission line.

The magnetic resonance of the structure is identified by comparing it with a closed ring resonator (CRR) of the same dimensions as stated in [33] and is shown in Fig. 4. The fundamental resonance of CRR is found to be at 4.365 GHz below which the SRR and ASSR show negative permeability (first) and permittivity resonances (second). The SRR of the same outer diameter and gap-width and excited with s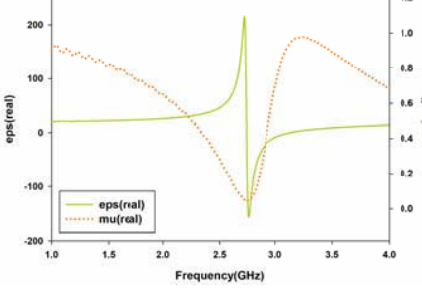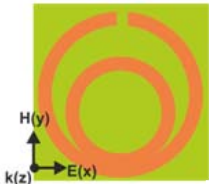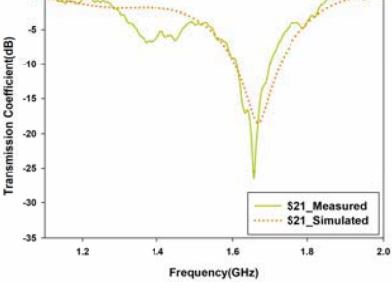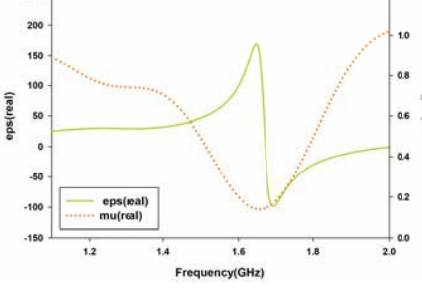imilar boundary conditions exhibit a lower resonance of 1.23 GHz. Compared to SRR and SD-SRR, the magnetic resonance of ASSR is at 1.63 GHz slightly greater which is attributed to the less capacitance effect after nullifying the distributed capacitance between the rings as explained in Section 2. However, the second resonance of ASSR is less than SRR and SD-SRR where both show the electrical resonance of the metamaterial structure. The higher-order mode which is rather inaccessible in the symmetric structure is brought closer to the fundamental mode by introducing asymmetry. The critical carving of the asymmetric parameter may create a strong coupling of these modes inducing high quality (Q) factor

Fano-resonance in succession. The variation in resonance for the asymmetry 'da' is depicted in Fig. 5. The asymmetric parameter $da = 3$ means that the inner ring is moved $3\,\text{mm}$ towards $+Y$ direction, and $da = -3$ indicates the displacement towards $-Y$ direction by $3\,\text{mm}$. SD-SRR is an SRR with minimum asymmetry, i.e., $da = 0$ and maximum Q. As the asymmetry increases, the Q of the structure decreases, and therefore ASSR is with a Q factor less than that of SD-SRR. The tuning of Q can be done by varying the asymmetry in the structure. Besides, the frequency variation thus by a change in capacitance of the structure with asymmetry is clear with the Fig. 5. Also, it is worth noticing that the resonance curve of ASSR shows very sharp resonances giving high Q which will facilitate the design of high-performance filters and sensors. The high Q-factor indicates less radiative and non-radiative losses due to the meta-particle.

The transmission properties of the metamaterial structure for the above electromagnetic polarization is measured experimentally in an anechoic chamber at normal incidence by two broadband horn antennas and a vector network analyzer PNA E8362B. The measured transmission spectra are

Table 1. Measured and simulated transmission coefficients and permittivity/permeability for incident wave polarizations (i), (ii), and (iii).

No	Incident Plane-wave Polarization	Transmission Characteristics	Permittivity and permeability
i			
ii			
iii			

depicted in Table 1 as case (i). The array of ASSR is placed in between two horn antennas such that the field vectors are oriented as in the polarization given in Fig. 3(a). The measured response and simulated resonant frequency response are in agreement within tolerable limits with acceptable manual errors due to the positioning of the array between antennas. A single fabricated unit cell of miniaturized ASSR has only a footprint of $0.163\lambda_0 \times 0.163\lambda_0$ sq.cm where λ_0 is the measured free-space wavelength corresponding to $1.63\,\mathrm{GHz}$.

The single split geometry of ASSR media which is considered an LC resonator does possess a high level of asymmetry. Therefore, it may result in magneto-electric coupling and cross polarizing behavior making it bianisotropic. Thus, the magnetic response of the unit cell is excited electrically as in case (iii) of Table 1. It gives a negative permittivity band above its plasma frequency. To investigate more into the resonant nature of ASSR, the responses for different polarizations of the incident electromagnetic wave of an electric field $\vec{E}$, magnetic field $\vec{H}$, and propagation vector $\vec{k}$ are listed in Table 1. The excitations given, simulated, and measured transmission coefficients and its permittivity/permeability have been figured out. To demonstrate the simulation and measurement setup, the arrangement is depicted in Fig. 6 for case (iii).
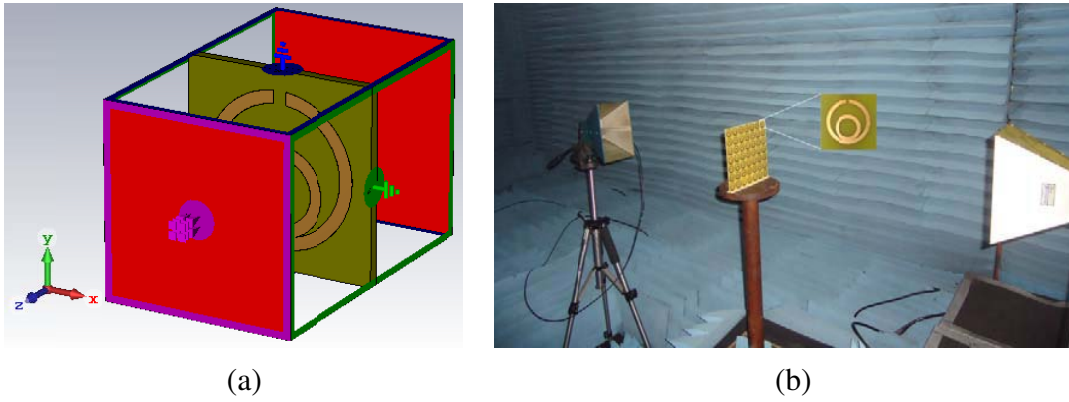

(a)   (b)

Figure 6. (a) Simulation and (b) measurement set up for polarization given in Table 1, case (iii).

The constitutive parameters of the material are extracted using the 3D EM simulation tool CST microwave studio for the incident polarizations for infinite periodic arrangement and boundary conditions based on Eqs. (4)–(6) where d is the unit cell dimension.

$$z = \pm\sqrt{\frac{(1 + S_{11})^2 + S_{21}^2}{(1 - S_{11})^2 + S_{21}^2}} \tag{4}$$

$$\eta = \frac{1}{k_0 d}\cos^{-1}\left[\frac{1}{2S_{21}}(1 - S_{11}^2 + S_{21}^2)\right] \tag{5}$$

$$\epsilon = \frac{\eta}{z} \quad \text{and} \quad \mu = \eta z \tag{6}$$

The ASSR magnetic resonance is very well proven by the permeability curve in case (i). The second resonance of ASSR is also investigated and depicted as case (ii). The electrical response is excited with the incident magnetic field giving a broader negative permittivity band at $2.5\,\mathrm{GHz}$. The ASSR response to the external magnetic field is less than an external electrical field as evident from the magnitudes of permittivity and permeability plots depicted in Table 1.

The macroscopic properties of the ASSR at resonance the absolute value of the total E field are plotted in Fig. 7. It is clear from the figures that the electric field is dominant in the vicinity of splits/gap of the ring. It mostly behaves as a spiral resonator where the major E-field component is stored by the distributed capacitance across the gap providing less radiation into space and high field confinement within the particle. So the asymmetric distribution of current increases the energy density within the volume. Hence the local field confinement across the gap is more for ASSR than an SRR of the same
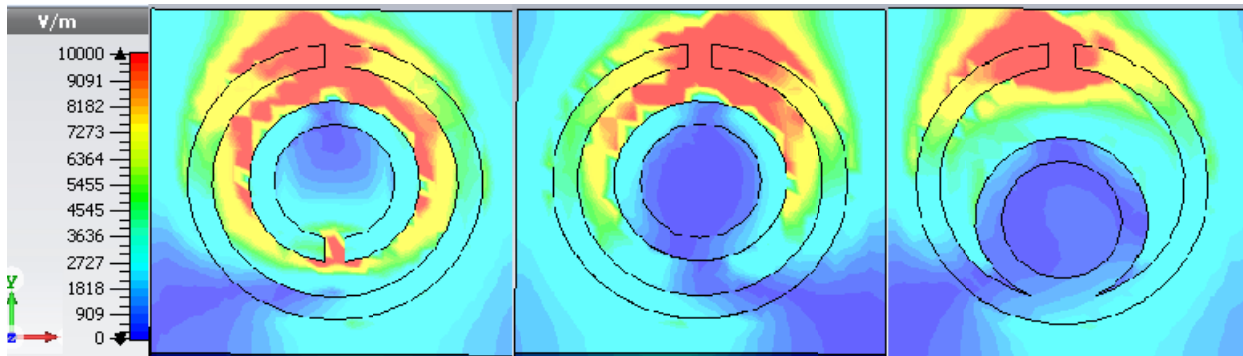
Figure 7. Electric field confinement of conventional SRR, single split double-ring SRR, and proposed ASSR.
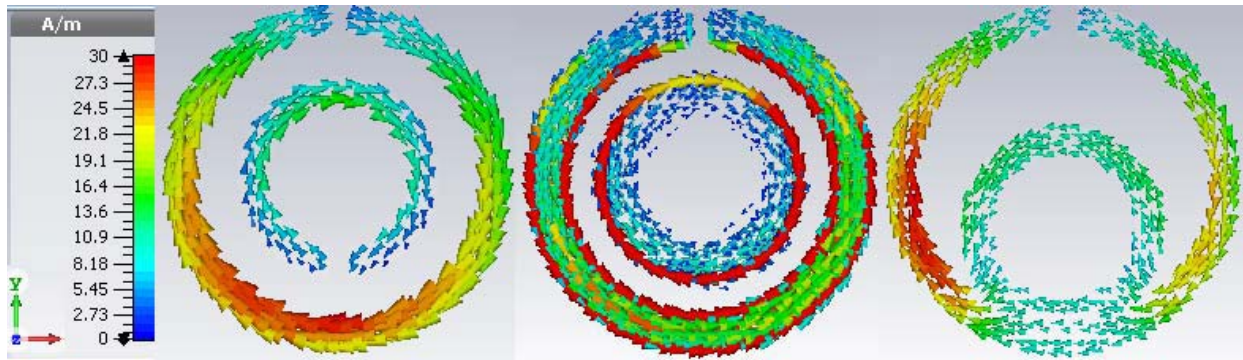

Figure 8. Surface current distribution of conventional SRR, single split double-ring SRR, and proposed ASSR.

dimension as evident in Fig. 7. Thus, it may be well suited for the sensor and RFID applications rather than SRR.

The current distribution at the resonance in Fig. 8 shows the anti-parallel loop currents through the inner and outer rings indicating the existence of negative permeability. The surface current distribution shows strong magnetic field localization in SD-SRR and variation in ASSR. Weakly nonlinear materials

Table 2. Comparison of different measured characteristics of SRR, SD-SRR, and ASSR for different polarizations in (i), (ii), and (iii).

Measured characteristics	Case (i)			Case (ii)			Case (iii)		
at resonance	SRR	SD-SRR	ASSR	SRR	SD-SRR	ASSR	SRR	SD-SRR	ASSR
Resonant frequency (GHz)	1.2437	1.4086	1.6275	3.388	3.239	2.7325	1.2315	1.4092	1.6495
$2:1$ VSWR Bandwidth (MHz)	32.6	25.7	47.6	520	357	228	51.2	75	118.5
Quality Factor (Q)	38.15	54.81	34.19	6.5	9.1	12	24.1	18.8	13.9
E-field maximum (V/m)	40940	35118	36908	9200	15244	22339	31669	29032	31466
Surface current(A/m)	31.7	91.3	31.6	13.6	51.2	107	30.3	100	119
mu^*/$eps^\#$ negative Bandwidth (MHz)	97.7^*	73.5^*	104.1^*	$866.5^\#$	$568.5^\#$	$399.5^\#$	$177^\#$	$258^\#$	$356^\#$
Magnitude of S_{21} (dB)	-13.15	-13.57	-16.35	-33.45	-29.86	-25.10	-13.97	-16.68	-18.25
Magnitude of S_{11} (dB)	-2.22	-1.83	-1.32	-0.18	-0.28	-0.48	-1.84	-1.34	-0.97

placed at the well-packed energy locations of ASSR may show considerable effects that will explore the manufacturing of active components for other applications too. The summary of different characteristics of SRR, SD-SRR, and ASSR is shown in Table 2 for reference.

The comparison of the proposed asymmetric single split resonator with already reported major resonators over the past decade is given in Table 3. It is well verified with the comparison table that the proposed resonator is comparable with major reported works in terms of bandwidth, quality factor, and size. The structure reported in [12, 34, 35] seems superior in terms of quality factor but compromising on complexity in structural fabrication, bandwidth, and size. Also, the proposed ASSR is a competent metamaterial component for [2] with high field localization. With enhanced field sites, sharp resonance, and bandwidth, the ASSR is the right candidate for advanced wireless communication systems and future sensor technologies used for the 5G communication network but not limited too.

Table 3. Comparison of proposed ASSR with different state-of-the-art metamaterial resonators.

Metamaterial Resonator	Frequency (GHz)	Bandwidth (%)	Quality Factor	Size
Split Ring Resonator [2]	1.2437	2.62	38.15	$0.125\lambda * 0.125\lambda * 0.007\lambda$
2D Cross Embedded Resonator [3]	2.34	1.7	58.5	$0.390\lambda * 0.137\lambda * 0.016\lambda$
Triangular Metamaterial Resonator [4]	8.8	12.5	8	$0.088\lambda * 0.088\lambda * 0.013\lambda$
S-shaped Metamaterial Resonator [5]	9	Not mentioned		$0.191\lambda * 0.103\lambda * 0.007\lambda$
Asymmetic Single Split Resonator [12]	6.31	0.47	221	$0.141\lambda * 0.141\lambda * 0.003\lambda$
CRLH Quad Band Resonator [34]	3.9	0.935	106.8	$0.215\lambda * 0.215\lambda * 0.020\lambda$
Asymmetric Dogbone shaped Resonator [35]	810	1.72	58	$0.486\lambda * 0.486\lambda * 0.00005\lambda$
Proposed ASSR	1.6275	2.92	34.19	$0.163\lambda * 0.163\lambda * 0.009\lambda$

4. CONCLUSION

A new uniplanar miniaturized asymmetric single split metamaterial to achieve negative permittivity/permeability is proposed in this paper. The ASSR structure is an asymmetric non-concentric ring resonator exhibiting high field confinement as compared to SRR, so it can be used for high-performance filter, sensor, and RFID systems for advanced communication services. The paper also discusses the cross-polarization effect and presents the constitutive parameters of ASSR for different incident polarizations with supporting simulation and measurement results. It can be used for single negative and/or double negative metamaterial applications with different polarization of the incident wave.

ACKNOWLEDGMENT

REFERENCES

1. Pendry, J. B., A. J. Robbins, D. J. Stewart, and W. J. Stewart, "Magnetism from conductors and enhanced nonlinear phenomena," *IEEE Trans. on Microwave Theory and Techniques*, Vol. 47, 2075–2084, 1999.
2. Smith, D. R., W. J. Padilla, D. C. Vier, S. C. Nemat-Nasser, and S. Schultz, "Composite medium with simultaneously negative permeability and permittivity," *Physical Review Letters*, Vol. 84, 4184–4187, 2000.
3. Zhang, J., H. Chen, L. Ran, Y. Luo, and J. A. Kong, "Two-dimensional cross embedded metamaterials," *PIERS Online*, Vol. 3, No. 3, 241–245, 2007.

4. Faruque, M. R. I., M. T. Islam, and N. Misran, "Design analysis of new metamaterial for EM absorption reduction," *Progress In Electromagnetics Research*, Vol. 124, 119–135, 2012.

5. Chen, H., L.-X. Ran, J. T. Huang-Fu, X. M. Zhang, K. S. Chen, T. M. Grzegorczyk, and J. A. Kong, "Magnetic properties of S-shaped split-ring resonators," *Progress In Electromagnetics Research*, Vol. 51, 231–247, 2005.

6. Zheludev, N. I., "The road ahead for metamaterials," *Science*, Vol. 328, 582–583, 2010.

7. Lee, J.-G. and J.-H. Lee, "Suppression of spurious radiations of patch antennas using split-ring resonators (SRRs)," *Microw. Opt. Technol. Lett.*, Vol. 48, 283–287, 2006.

8. Panda, P. K. and D. Ghosh, "Isolation, and gain enhancement of patch antennas using EMNZ superstrate," *Int. Journal of Electronics and Communications*, Vol. 86, 164–170, 2018.

9. Anila, P. V., V. P. Sarin, M. Manoj, M. Remsha, and P. Mohanan, "Broadband non-resonant split ring resonator-based artificial high dielectric substrate," *Int. Journal of Electronics and Communications*, Vol. 117, 153095, 2020.

10. Fedotov, V. A., M. Rose, S. L. Prosvirnin, N. Papasimakis, and N. I. Zheludev, "Sharp trapped-mode resonances in planar metamaterials with a broken structural symmetry," *Phys. Rev. Lett.*, Vol. 99, 147401, 2007.

11. Al-Naib, I. A. I., C. Jansen, and M. Koch, "Thin-film sensing with planar asymmetric metamaterial resonators," *App. Phys. Lett.*, Vol. 93, 083507, 2008.

12. Al-Naib, I. A. I., C. Jansen, and M. Koch, "High Q-factor metasurfaces based on miniaturized asymmetric single split resonators," *Appl. Phys. Lett.*, Vol. 94, 153505, 2009.

13. Al-Naib, I., R. Singh, C. Rockstuhl, F. Lederer, S. Delprat, et al., "Excitation of a high-Q subradiant resonance mode in mirrored single-gap asymmetric split ring resonator terahertz metamaterials," *Appl. Phys. Lett.*, Vol. 101, 071108, 2012.

14. Li, Y., Z. Zhao, Z. Tang, and Y. Yin, "A low-profile, dual-band filtering antenna with high selectivity for 5G sub-6 GHz applications," *Microw. Opt. Technol. Lett.*, Vol. 61, 2282–2287, 2019.

15. Selvaraju, R., M. H. Jamaluddin, M. R. Kamarudin, J. Nasir, and M. H. Dahri, "Complementary split ring resonator for isolation enhancement in 5G communication antenna array," *Progress In Electromagnetics Research C*, Vol. 83, 217–228, 2018.

16. Abdelgwad, A. H. and M. Ali, "Capacity and efficiency improvement of MIMO antenna systems for 5G handheld terminals," *Progress In Electromagnetics Research C*, Vol. 104, 269–283, 2020.

17. Huang, M., Y. Cheng, Z. Cheng, H. Chen, X. Mao, and R. Gong, "Based on graphene tunable dual-band terahertz metamaterial absorber with wide-angle," *Optics Communications*, Vol. 415, 194–201, 2018.

18. Zou, H. and Y. Cheng, "Design of a six-band terahertz metamaterial absorber for temperature sensing application," *Optical Materials*, Vol. 88, 674–679, 2019.

19. Li, W. and Y. Cheng, "Dual-band tunable terahertz perfect metamaterial absorber based on strontium titanate (STO) resonator structure," *Optics Communications*, Vol. 462, 125265, 2020.

20. Cheng, Y., J. Fan, H. Luo, and F. Chen, "Dual-band and high-efficiency circular polarization convertor based on anisotropic metamaterial," *IEEE Access*, Vol. 8, 7615–7621, 2020.

21. Fan, J. and Y. Cheng, "Broadband high-efficiency cross-polarization conversion and multi-functional wavefront manipulation based on chiral structure metasurface for terahertz wave," *J. of Physics D: Applied Physics*, Vol. 53, No. 2, 2020.

22. Cheng, Y., H. Luo, and F. Chen, "Broadband metamaterial microwave absorber based on asymmetric sectional resonator structures," *J. Appl. Phys.*, Vol. 127, 214902, 2020.

23. Chen, F., Y. Cheng, and H. Luo, "A broadband tunable terahertz metamaterial absorber based on single-layer complementary Gammadion-shaped graphene," *Materials*, Vol. 13, 860, 2020.

24. Cheng, Y., F. Chen, and H. Luo, "Triple-band perfect light absorber based on hybrid metasurface for sensing application," *Nanoscale Res. Lett.*, Vol. 15, 103, 2020.

25. Cheng, Y., H. Zhao, and C. Li, "Broadband tunable terahertz metasurface absorber based on complementary-wheel-shaped graphene," *Optical Materials*, Vol. 109, 110369, 2020.

26. Wang, Q. and Y. Cheng, "Compact and low-frequency broadband microwave metamaterial absorber based on meander wire structure loaded resistors," *AEU-International Journal of Electronics and Communications*, Vol. 120, 153198, 2020.

27. Keshavarz, S. and N. Nozhat, "Dual-band Wilkinson power divider based on composite right/left-handed transmission lines," *Proceed. of 13th International Conference on Electrical Engineering/Electronics, Computer, Telecommunications and Information Technology (ECTI-CON)*, 1–4, Chiang Mai, 2016.

28. Keshavarz, S., A. Abdipour, A. Mohammadi, and R. Keshavarz, "Design and implementation of low loss and compact microstrip triplexer using CSRR loaded coupled lines," *AEU-International Journal of Electronics and Communications*, Vol. 111, 152913, 2019.

29. Keshavarz, R., M. Danaeian, M. Movahhedi, and A. Hakimi, "A compact dual-band branch-line coupler based on the interdigital transmission line," *Proceed. of 19th Iranian Conference on Electrical Engineering*, Tehran, 2011.

30. Keshavarz, R., Y. Miyanaga, M. Yamamoto, T. Hikage, and N. Shariati, "Metamaterial-inspired quad-band notch filter for LTE band receivers and WPT applications," *Proceed. of 2020 XXXIIIrd General Assembly and Scientific Symposium of the International Union of Radio Science*, 1–4, Rome, Italy, 2020.

31. Keshavarz, R., A. Mohammadi, and A. Abdipour, "A quad-band distributed amplifier with E-CRLH transmission line," *IEEE Transactions on Microwave Theory and Techniques*, Vol. 61, No. 12, 4188–4194, 2013.

32. Kulkarni, J., "Multi-band printed monopole antenna conforming bandwidth requirement of GSM/WLAN/WiMAX standards," *Progress In Electromagnetics Research Letters*, Vol. 91, 59–66, 2020.

33. Aydin, K., I. Bulu, K. Guven, M. Kafesaki, C. M. Soukoulis, and E. Ozbay, "Investigation of magnetic resonances for different split-ring resonator parameters and designs," *New Journal of Physics*, Vol. 7, 168, 2005.

34. Daw, A. F., P. A. Fawzey, and M. N. Adly, "Quad-band resonator depends on CRLH/D-CRLH structures," *Microwaves & RF*, October 2019.

35. Xie, Q., G. Dong, B. Wang, et al., "High-Q Fano resonance in terahertz frequency based on an asymmetric metamaterial resonator," *Nanoscale Res. Lett.*, Vol. 13, 294, 2018.